Light-emission mechanism of Si-MOS tunnel junctions

Y. Uehara, J. Watanabe,* S. Fujikawa,† and S. Ushioda
Research Institute of Electrical Communication, Tohoku University, Sendai 980-77, Japan
(Received 11 July 1994; revised manuscript received 18 October 1994)

The light-emission mechanism of Si-MOS (metal-oxide-semiconductor) junctions has been investigated. Si/SiO_2/metal (Al or Au) MOS junctions with extremely smooth interfaces were fabricated by taking advantage of the well-developed Si processing technology. The observed light-emission spectra can be accounted for by the current fluctuation theory of light-emitting tunnel junctions [B. Laks and D. L. Mills, Phys. Rev. B 20, 4962 (1979)]. There are two channels of light emission: the direct emission from the fluctuation of the tunneling current and the indirect emission that arises from the scattering (by surface roughness) of surface-plasmon polaritons generated by the fluctuating tunnel current. The light from the $Si/SiO_2/Al$ junction arises mainly from the direct emission from the fluctuating current. The light from the $Si/SiO_2/Au$ junction contains both the direct and indirect emissions with approximately equal strengths. The direct and indirect emissions have comparable strength in our junctions, because our Si-based junctions are extremely smooth and the indirect emission is much weaker than in the junctions used in earlier studies.

I. INTRODUCTION

The visible light emission associated with electron tunneling was reported by Lambe and McCarthy in 1975.[1] They fabricated tunnel junctions that consisted of metal-oxide-metal (MOM) multilayers, and observed visible light emission by applying a few volts of bias voltage across the oxide layer. The light-emitting tunnel junctions (LETJ's) are interesting not only from the practical point of view as display devices but also from the fundamental physical point of view, because they offer an opportunity to investigate electron tunneling phenomena through optical means.

Lambe and McCarthy proposed a mechanism for the light emission in their original paper.[1] According to their proposal, surface-plasmon polaritons (SPP's) in the junction are excited first by inelastically tunneling electrons, and then they decay into external light by scattering from surface roughness of the junction. A theoretical formulation of the proposal was developed by Laks and Mills.[2] They formulated the light-emission process by considering the radiation from a fluctuating tunnel current embedded in the oxide barrier. They found that there are two channels of light emission from the tunneling current. In addition to the surface-roughness-mediated indirect emission channel proposed by Lambe and McCarthy, there exists a direct emission channel from the fluctuating tunnel current. This direct emission is very interesting to explore, because its spectrum should directly reflect the spectrum of the fluctuating current, which has a quantum-mechanical origin. However, the indirect emission that is mediated by surface roughness is often much stronger than the direct emission in the usual junctions. Thus it is not easy to isolate the direct emission from the total emission spectrum. To reduce the indirect emission and identify the direct emission unambiguously, it would be necessary to fabricate LETJ's whose surface is extremely smooth on the scale of a few angstroms.[3] Furthermore, the electrical properties of the junction must be very well defined, so that the power spectrum of the tunneling-current fluctuation can be calculated rigorously.[4]

Recently Si-MOS (metal-oxide-semiconductor) junctions ($Si/SiO_2/Al$ and $Si/SiO_2/Au$) with stable and reproducible electrical properties were fabricated by use of the well-developed Si-processing technology, and visible light emission associated with electron tunneling was observed.[5] The Si-MOS junction has a very smooth surface, and the oxide barrier thickness and its dielectric properties are well controlled. Thus the relative contribution from the direct emission is strong, and the power spectrum of the tunneling current can be calculated reliably from the measured electrical properties of the junction.

In the present work we compare the observed light-emission spectra of Si-MOS junctions[5] with the theoretical predictions. We calculated the current fluctuation spectra of the junctions and inserted them as the source term in the light-emission theory.[3] We found that the emission from the $Si/SiO_2/Al$ junction is mainly from the direct emission. In contrast, the indirect emission mediated by surface roughness is comparable to the direct emission in the $Si/SiO_2/Au$ junction. This difference between the $Si/SiO_2/Al$ and $Si/SiO_2/Au$ junctions arises from the difference in the amplitude of the SPP that is excited at the interface between the metal electrode and the SiO_2 barrier.

In Sec. II a brief summary of the light-emission theory is presented, and the experimental details are described in Sec. III. The experimental and theoretical results are presented in Sec. IV. The emission mechanism is discussed in Sec. V, and Sec. VI is the conclusion.

II. THEORY

Light emission from LETJ's is calculated by considering the radiation from a fluctuating-current source em-

bedded in an n-layered structure with $n-1$ interfaces as shown in Fig. 1.[2,3] z_m $(m=1-n-1)$ is the z position of the mth average interface plane and $\zeta_m(\mathbf{x}_p)$ is the roughness profile function of the mth interface. $\mathbf{x}_p$ is a two-dimensional vector in the x-y plane. Thus $\langle\zeta_m(\mathbf{x}_p)\rangle=0$ where $\langle\cdots\rangle$ means a statistical average over the interface plane. d_m and ε_m are the mean thickness and the dielectric function of the mth layer, respectively. The effect of the roughness is included in the theory as a perturbative term in the Maxwell equation.[2,3] The Si-MOS junction is modeled by a four-layered structure that consists of an n-type Si layer with a semi-infinite thickness, a SiO_2 layer for the tunneling barrier, a metal layer for the counterelectrode, and a vacuum layer with semi-infinite thickness above the junction.

We assume that the emitted light is observed in the x-z plane. Then the final expressions for the radiated power with p and s polarizations are given by[3]

$$\left[\frac{dW}{d\Omega\,d\omega\,dt}\right]_{p\ \mathrm{pol}}=A\frac{\varepsilon_0^{3/2}\omega^4\cos^2\theta_0}{8\pi c^5}\sum_{\mu=x,z}\int dz'dz''\gamma_{\mu z}(\mathbf{k}_p^{(0)},\omega|z')^*\gamma_{\mu z}(\mathbf{k}_p^{(0)},\omega|z'')J_{zz}(\mathbf{k}_p^{(0)},\omega|z'z'')$$
$$+A\frac{\varepsilon_n^{3/2}\omega^8\cos^2\theta_0}{512\pi^5c^9}\sum_{\mu=x,z}\sum_{\eta\eta'}\sum_{mm'}\int d^2Q_p\,dz'dz''\Delta\varepsilon_m^*\Delta\varepsilon_{m'}\gamma_{\mu\eta}(\mathbf{k}_p^{(0)},\omega|z_m^+)^*\gamma_{\mu\eta'}(\mathbf{k}_p^{(0)},\omega|z_{m'}^+)$$
$$\times\zeta_m(\mathbf{k}_p^{(0)}-\mathbf{Q}_p)^*\zeta_{m'}(\mathbf{k}_p^{(0)}-\mathbf{Q}_p)$$
$$\times d_{\eta z}(\mathbf{Q}_p,\omega|z_m^-z')^*d_{\eta' z}(\mathbf{Q}_p,\omega|z_{m'}^-z'')J_{zz}(\mathbf{Q}_p,\omega|z'z'')\ , \tag{1}$$

$$\left[\frac{dW}{d\Omega\,d\omega\,dt}\right]_{s\ \mathrm{pol}}=A\frac{\varepsilon_n^{3/2}\omega^4\cos^2\theta_0}{8\pi c^5}\int dz'dz''\gamma_{yz}(\mathbf{k}_p^{(0)},\omega|z')^*\gamma_{yz}(\mathbf{k}_p^{(0)},\omega|z'')J_{zz}(\mathbf{k}_p^{(0)},\omega|z'z'')$$
$$+A\frac{\varepsilon_n^{3/2}\omega^8\cos^2\theta_0}{512\pi^5c^9}\sum_{\eta\eta'}\sum_{mm'}\int d^2Q_p\,dz'dz''\Delta\varepsilon_m^*\Delta\varepsilon_{m'}\gamma_{y\eta}(\mathbf{k}_p^{(0)},\omega|z_m^+)^*\gamma_{y\eta'}(\mathbf{k}_p^{(0)},\omega|z_{m'}^+)$$
$$\times\zeta_m(\mathbf{k}_p^{(0)}-\mathbf{Q}_p)^*\zeta_{m'}(\mathbf{k}_p^{(0)}-\mathbf{Q}_p)$$
$$\times d_{\eta z}(\mathbf{Q}_p,\omega|z_m^-z')^*d_{\eta' z}(\mathbf{Q}_p,\omega|z_{m'}^-z'')J_{zz}(\mathbf{Q}_p,\omega|z'z'')\ , \tag{2}$$

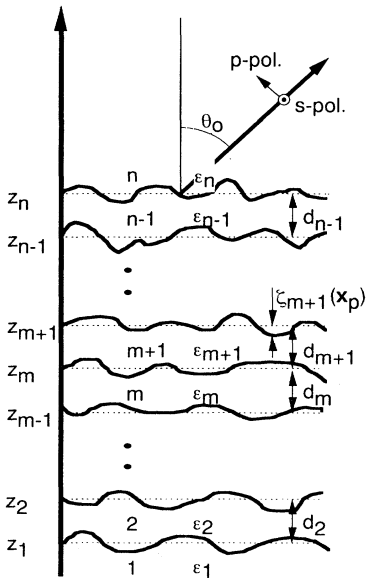

FIG. 1. Model structure for the theoretical calculation. Light emission is formulated as a radiation process from a current source embedded in the n-layered structure. The two unit vectors denoted by p-pol. and s-pol. define the directions of the electric field for the p- and s-polarized light.

where the directions of the electric field of p- and s-polarized light are defined in Fig. 1, A is the area of the junction, θ_0 is the radiation angle measured from the surface normal, $\mathbf{k}_p^{(0)}$ is the component of the light wave vector parallel to the surface, and $d_{\mu\nu}(\mathbf{k},\omega|zz')$ and $\gamma_{\mu\nu}(\mathbf{k},\omega|z')$ are the electromagnetic Green's functions for the structure of Fig. 1 with flat interfaces $[\zeta_m(\mathbf{x}_p)=0]$. Their explicit forms are found in Ref. 6. $\Delta\varepsilon_m$ is defined by $\Delta\varepsilon_m=\varepsilon_m-\varepsilon_{m+1}$. $\zeta_m(\mathbf{k})$ is the two-dimensional Fourier transform of $\zeta_m(\mathbf{x}_p)$. Here we assume a Gaussian distribution for the correlation function of roughness:

$$\langle\zeta_m(\mathbf{k})^*\zeta_{m'}(\mathbf{k})\rangle=A\pi a^2\delta^2\exp(-\tfrac{1}{4}a^2|\mathbf{k}|^2)\delta_{mm'}\ , \tag{3}$$

where a is the autocorrelation distance of surface roughness and δ is the root-mean-squared amplitude of roughness. The Kronecker symbol $\delta_{mm'}$ in Eq. (3) refers to the assumption that there is no correlation between corrugated profiles $\zeta_m(\mathbf{x}_p)$ and $\zeta_{m'}(\mathbf{x}_p)$ at different interfaces. $J_{zz}(\mathbf{Q}_p,\omega|z'z'')$ is defined by

$$J_{zz}(\mathbf{Q}_p,\omega|z,z')=\int d^2(\mathbf{x}_p''-\mathbf{x}_p')\frac{1}{(2\pi)^2}e^{i\mathbf{Q}_p\cdot(\mathbf{x}_p''-\mathbf{x}_p')}$$
$$\times\langle J_z(\mathbf{x}',\omega)^*J_z(\mathbf{x}'',\omega)\rangle\ , \tag{4}$$

where $J_z(\mathbf{x},\omega)$ is the tunneling-current density at position

$\mathbf{x}$ in the junction, and $\langle \cdots \rangle$ means a statistical average.[2]

The first terms of both Eqs. (1) and (2) represent the direct emission from the fluctuating tunnel current, and they do not depend on the surface roughness. The light with s polarization is not radiated directly from the fluctuating current, because γ_{yz} of Eq. (2) is zero.[6] The second terms of Eqs. (1) and (2) physically correspond to the process in which the SPP's excited by the fluctuating current emit light by scattering from the surface roughness. The information on the properties of the SPP's that depend on the constituent materials is contained in $d_{\mu\nu}(\mathbf{k}_p,\omega|zz')$.

According to Laks and Mills,[2] the current-current correlation $\langle J_z(\mathbf{x}',\omega)^* J_z(\mathbf{x}'',\omega)\rangle$ in Eq. (4) can be written in the form

$$\langle J_z(\mathbf{x}',\omega)^* J_z(\mathbf{x}'',\omega)\rangle = |I(\omega)|^2 G(\mathbf{x},\mathbf{x}') , \tag{5}$$

where $G(\mathbf{x},\mathbf{x}')$ is given by the phenomenological form[2]

$$G(\mathbf{x},\mathbf{x}') = \frac{\exp(-|\mathbf{x}-\mathbf{x}'|/\xi_0)}{\pi\xi_0^2 A}\Delta(z,z') . \tag{6}$$

$\Delta(z,z')$ will be taken to be unity only in the barrier, and the autocorrelation distance of the tunneling electron ξ_0 is assumed to be 10 nm following Ref. 2. The specific functional form of $G(\mathbf{x},\mathbf{x}')$ has only a weak influence on the calculated emission spectra. Thus we can make these assumptions about $\Delta(z,z')$ and ξ_0 without affecting the calculated spectra in any significant way. $|I(\omega)|^2$ is the power spectrum of the current fluctuation defined by the Fourier transform of the correlation function of the tunneling current:[7]

$$\begin{aligned}|I(\omega)|^2 &= \int_{-\infty}^{+\infty} dt \langle \hat{I}(t)^+ \hat{I}(0)\rangle e^{-i\omega t} \\ &= 2\pi\left[\frac{e}{\hbar}\right]^2 \sum_{k,q,s} |T_{kq}|^2 \left\{ |\langle q|c_{q,s}^\dagger c_{k,s}|k\rangle|^2 \delta\left[\frac{E_k-E_q}{\hbar}-\omega\right] - |\langle k|c_{k,s}^\dagger c_{q,s}|q\rangle|^2 \delta\left[\frac{E_q-E_k}{\hbar}-\omega\right]\right\} .\end{aligned} \tag{7}$$

Here $\hat{I}$ is the quantum-mechanical tunneling-current operator represented by

$$\hat{I} = \frac{ie}{\hbar}\sum_{k,q,s}\left(T_{kq}c_{q,s}^\dagger c_{k,s} - T_{kq}^* c_{k,s}^\dagger c_{q,s}\right) , \tag{8}$$

where T_{kq} is the tunneling matrix element between the state k in the source electrode and the state q in the counterelectrode. $c_{i,s}^\dagger$ and $c_{i,s}$ are the creation and annihilation operators of the electron, respectively. The subscript s represents the spin states.

By use of the WKB method for calculating the electron wave functions, the tunneling matrix element can be written[4]

$$|T_{kq}|^2 = \left[\frac{\hbar^2}{2m^*}\right]^2 \frac{k_\perp}{L_k}\frac{q_\perp}{L_q}\exp\left[-\int dz|K_\perp(z,k_\parallel,E_k)|\right] \times \exp\left[-\int dz|K_\perp(z,q_\parallel,E_q)|\right] , \tag{9}$$

where m^* is the effective mass of the electron in the tunneling barrier, L_j $(j=k,q)$ is the normalization constant of the electron wave function for the j state, $k_\perp$ and $k_\parallel$ ($q_\perp$ and $q_\parallel$) are the wave-vector components perpendicular and parallel to the junction interface, respectively. $K_\perp$ is the component of the electron wave vector in the barrier perpendicular to the junction interface. It is given by

$$K_\perp(z,k_\parallel,E) = \frac{\sqrt{2m^*}}{\hbar}\left[V(z)-E+\frac{\hbar^2}{2m^*}k_\parallel^2\right]^{1/2} . \tag{10}$$

Here $V(z)$ is the barrier potential and z is the coordinate of the axis perpendicular to the junction interfaces.

By substituting Eq. (9) into Eq. (7) we finally obtain the following expression for the power spectrum of the current fluctuation:

$$\begin{aligned}|I(\omega)|^2 = \frac{e^2 A m_\parallel}{2\pi^2\hbar^3} &\times \int dE \int dE_\parallel \exp\left[-\int dz|K_\perp(z,k_\parallel,E)|\right] \\ &\times \exp\left[-\int dz|K_\perp(z,k_\parallel,E-\hbar\omega)|\right] ,\end{aligned} \tag{11}$$

where A is the area of the junction. $m_\parallel$ is the effective mass of the electron moving parallel to the junction in the source electrode from which the tunneling electrons are injected into the barrier, and $E_\parallel = (\hbar^2/2m_\parallel)k_\parallel^2$.

Let us transform Eq. (11) into a more suitable form for the Si-MOS junction. All the light-emission measurements were carrier out in the Fowler-Nordheim tunneling regime[5] where Eq. (11) can be simplified further to the form

$$|I(\omega)|^2 = \frac{e^3 A}{4\pi^2\hbar\phi_B}\left[\frac{m_\parallel}{m^*}\right]|E_{ox}|^2\left\{\left[\frac{\hbar\omega}{e\phi_B}+1\right]^{1/2}+1\right\}^{-2}\exp\left[-\frac{2\sqrt{2m^*}(e\phi_B)^{3/2}}{3\hbar e|E_{ox}|}\left\{\left[\frac{\hbar\omega}{e\phi_B}+1\right]^{3/2}+1\right\}\right] . \tag{12}$$

E_{ox} is the electric field in the barrier, and ϕ_B is the tunneling barrier height through which the tunneling electrons are injected into the barrier. As expected at $\omega=0$, $|I(0)|^2$ becomes the product of the elementary charge e and the Fowler-Nordheim tunneling current:

$$I=\frac{e^3A}{16\pi^2\hbar(e\phi_B)}\left[\frac{m_{\parallel}}{m^*}\right]|E_{ox}|^2 \times\exp\left[-\frac{4(2m^*)^{1/2}(e\phi_B)^{3/2}}{3\hbar e|E_{ox}|}\right]. \quad (13)$$

To carry out the computation of Eq. (12), we need to obtain ϕ_B and E_{ox}. For this purpose we consider the energy diagrams of the Si-MOS junction illustrated in Fig. 2: (a) and (b) correspond to the two biasing conditions of the metal electrode, negative and positive, respectively, relative to the Si substrate. We define the sign of the bias voltage V_{app} as positive when the metal is biased positively with respect to the Si substrate. The origin of the z axis is taken at the interface between the metal layer and the oxide layer.

For $V_{app}<0$, ϕ_B corresponds to the barrier height at the interface of the metal layer and the oxide layer. Since no band bending occurs in the metal, ϕ_B is the energy difference between the electron affinity of SiO_2 and the work function of the metal ($\phi_B=\phi_{Bm}$). In the numerical calculation of Eq. (12), the value of ϕ_{Bm} is taken from the literature (see the caption for Table I). For $V_{app}>0$, from the geometrical consideration of Fig. 2(b), ϕ_B is

$$\phi_B=\phi_{Bs}+\frac{k_BT}{e}\ln\left[\frac{N_C}{N_D}\right]-\psi_s\ , \quad (14)$$

where ϕ_{Bs} is the difference in electron affinity between SiO_2 and Si. $(k_BT/e)\ln(N_C/N_D)$ is the energy difference between the Fermi level and the bottom of the conduction band of Si,[8] and ψ_s is the surface potential. N_C and N_D are the effective density of states in the conduction band the donor impurity density, respectively.

As we will describe later, ϕ_{Bs} and N_C are obtained from the literature and N_D is determined experimentally. In order to calculate ϕ_B by Eq. (14), one needs to know the surface potential ψ_s. It has a finite value of ψ_{s0} even at the zero bias condition ($V_{app}=0$). The main origin of ψ_{s0} for the Si(100)-MOS junction with a thermally formed SiO_2 barrier is the oxide charge.[8] If we represent the distribution of the charge in the oxide layer by $\rho(z)$, the flat-band condition $\psi_s=0$ is attained at the bias voltage of

$$V_{FB}=\phi_{ms}-\frac{1}{\varepsilon_{ox}}\int_0^{d_{ox}}z\rho(z)dz\ , \quad (15)$$

where ϕ_{ms} is the work-function difference between Si and the metal, and ε_{ox} is the static dielectric constant of SiO_2. When the surface potential has a finite value, the z component of the electric field at the interface of Si and the oxide layer on the oxide side $E(\psi_s)$ is given by[8]

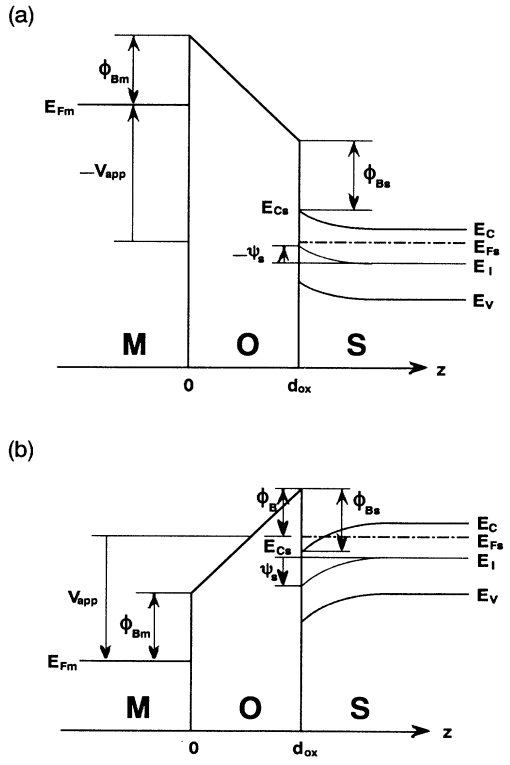

FIG. 2. Potential diagram of the electron in an n-type Si-MOS junction. (a) and (b) correspond to the biasing conditions with the metal negative and positive with respect to the Si substrate.

TABLE I. Parameters used in the theoretical calculations. m_0 is the free-electron mass.

	$Si/SiO_2/Al$	$Si/SiO_2/Au$
ϕ_m	4.1 eV[a]	5.0 eV[a]
χ_s	4.05 eV[a]	4.05 eV[a]
χ_{ox}	0.9 eV[a]	0.9 eV[a]
m^*	$0.33m_0$[b]	$0.45m_0$[b]
$m_{\parallel}$ ($V_{app}>0$)	$0.19m_0$[a]	$0.19m_0$[a]
$m_{\parallel}$ ($V_{app}<0$)	$1.00m_0$[b]	$0.0002m_0$[b]
ε_s	11.9[a]	11.9[a]
ε_{ox}	3.9[a]	3.9[a]
N_C	2.85×10^{19} cm^{-3}[a]	2.85×10^{19} cm^{-3}[a]
n_i	1.455×10^{10} cm^{-3}[a]	1.455×10^{10} cm^{-3}[a]
d_{ox}	6.6 nm[c]	5.9 nm[c]
N_D	6.65×10^{18} cm^{-3}[c]	5.95×10^{18} cm^{-3}[c]
V_{FB}	0.20 V[c]	0.0018 V[c]
T	300 K	300 K

[a]Reference 8.
[b]Determined to fit the theoretical I-V characteristics of the junctions to the experimental data. The details are described in Ref. 5.
[c]Obtained by C-V measurements.

$$E(\psi_s)=\pm\frac{(2\varepsilon_s N_D k_B T)^{1/2}}{\varepsilon_{ox}} \times\left\{\left[e^{e\psi_s/k_BT}-\frac{e\psi_s}{k_BT}-1\right]+\frac{n_i^2}{N_D^2}\left[e^{-e\psi_s/k_BT}+\frac{e\psi_s}{k_BT}-1\right]\right\}^{1/2}, \quad (16)$$

with a positive sign in front for $\psi_s>0$ and a negative sign for $\psi_s<0$. n_i is the intrinsic carrier density for the Si layer and its value is obtained from the literature.

Here we make a reasonable assumption to proceed in the calculation; that is, we assume that $\rho(z)$ is fixed and does not depend on the bias voltage.[8] Then the bias voltage V_{app} is given by

$$V_{app}=E(\psi_s)d_{ox}+\psi_s+V_{FB} . \quad (17)$$

As described in Sec. IV, V_{FB} is obtained experimentally for each individual junction used. Therefore one can calculate ψ_s as a function of V_{app} from Eq. (17).

Typical V_{FB} of our junctions is a few tenths of a volt or less as shown in Table I. This means that the electric-field strength created by the oxide charge is very weak in comparison to that created by the biasing voltage for light-emission measurements (it is above 6 V as described below). Thus E_{ox} is obtained by dividing the potential difference between the right- and left-hand sides of the barrier layer by the thickness d_{ox} of the barrier layer. The energy difference is seen from Fig. 2 to be

$$V_{app}+\phi_{Bs}-\phi_{Bm}+(k_BT/e)\ln(N_C/N_D)-\psi_s .$$

Thus E_{ox} is given by

$$E_{ox}=\left[V_{app}+\phi_{Bs}-\phi_{Bm}+\frac{k_BT}{e}\ln\left[\frac{N_C}{N_D}\right]-\psi_s\right]\Big/d_{ox} , \quad (18)$$

with ψ_s determined by Eq. (17).

III. EXPERIMENT

Figure 3 illustrates the cross-sectional view of the Si-MOS junction that we fabricated on a commercially available p-type Si(100) wafer. It consists of a highly doped n-type layer, a thin SiO_2 layer around 6 nm thick, and a metallic counterelectrode layer (Al or Au). The light emitted from the junction at 60° from the surface normal was observed with a combination of a spectrograph and an optical multichannel detector. The relative sensitivity of the spectrograph system as a function of the wavelength was calibrated with a standard lamp before the measurements, and the spectrum ranging from 460 to 810 nm was taken in a single exposure with a resolution of 27 nm. All the optical measurements were performed at room temperature. The details of the fabrication process of the junction and the experimental setup for the optical measurements were described in our previous publication.[5]

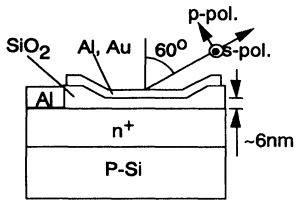

FIG. 3. Cross-sectional view of the Si-MOS junction. The Al electrode on the n-type layer is for the electrical contact.

IV. RESULTS

A. Experimental results

Figure 4 shows the emission spectra from a $Si/SiO_2/Al$ junction. The solid curves are the experimental data[5] and the dashed curves are the theoretical results. Figure 4(a) is the $V_{app}=+6.5$ V and Fig. 4(b) is for the $V_{app}=-8.0$ V. The thickness of the Al layer was 24.0 nm. By comparing Figs. 4(a) and 4(b) we see that the spectral shapes show no bias-polarity dependence.

The polarization of the emitted light was measured. We found that almost all of the emitted light is p polarized. By direct numerical comparison the intensity ratio of the s-polarized light to the p-polarized light was $\frac{1}{55}$.

Figure 5 shows the emission spectra from a $Si/SiO_2/Au$ junction. The solid and dashed curves are the experimental data[5] and the theoretical results, respectively. The bias voltage was -12.5 V. The thickness of the Au layer was 35.2 nm. By comparing Figs. 4 and 5, we see that there is a difference in the spectral shape be-

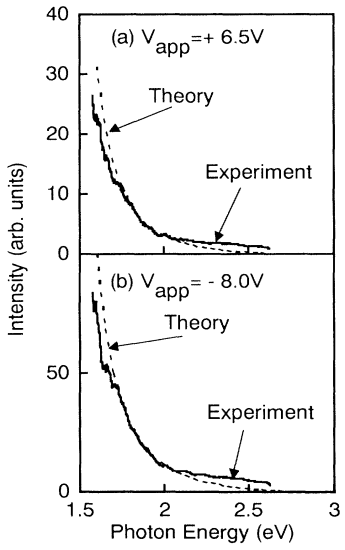

FIG. 4. Light-emission spectra from a $Si/SiO_2/Al$ junction. (a) is for $V_{app}=+6.5$ V and (b) is for $V_{app}=-8.0$ V. The solid curves and the dashed curves correspond to the experimental and theoretical results, respectively.

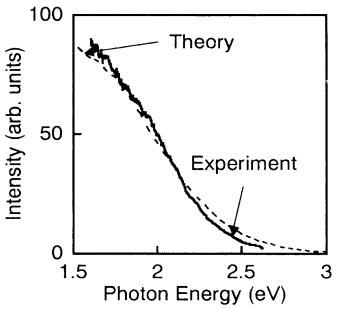

FIG. 5. Light-emission spectra from a $Si/SiO_2/Al$ junction. The bias voltage V_{app} is -12.5 V. The solid curves and the dashed curves correspond to the experimental and theoretical results, respectively.

tween the two junctions with Al and Au counterelectrodes, especially around the photon energy of 2 eV.

B. Comparison with the theory

Now let us compare the experimental results with the predictions of the theory described in Sec. II. The parameters that determine the tunneling characteristics are tabulated in Table I for the junctions of Figs. 4 and 5. As we have described in our previous paper,[5] the donor concentration N_D, the thickness of the oxide layer d_{ox}, and the flatband voltage V_{FB} were determined from the measurement of the junction capacitance as a function of the applied voltage (C-V measurements). Other parameters were obtained from the literature cited in Table I. The validity of these parameters was confirmed by comparing the observed I-V curves with the calculated Fowler-Nordheim tunneling current.[5] Excellent agreement was obtained between them.

The solid curves of Fig. 6 are the current fluctuation spectra calculated by Eq. (12): Figs. 6(a) and 6(b) correspond to the biasing conditions of $V_{app}=+6.5$ and -8.0 V, respectively. No clear difference in shape is seen between Figs. 6(a) and 6(b). Both spectra decrease exponentially toward the high-frequency side without showing any prominent feature. Similar results were obtained for the other junctions.

To proceed to the next step of the calculation [Eqs. (1) and (2)], we need the dielectric constants ε_m and the statistical properties of the interface roughness [a and δ in Eq. (3)]. The dielectric constants for Al, Au, Si, and SiO_2 were obtained from Ordal *et al.*,[9] Johnson and Christy,[10] Edwards,[11] and Philipp.[12] The autocorrelation distance and the root-mean-squared amplitude of roughness were estimated to be $a=20$ nm and $\delta=1.3$ nm as described in the next section.

By using the parameters specified above, the dashed curves in Figs. 4 and 5 were calculated. Each theoretical curve is normalized to the corresponding experimental curve at the photon energy of 1.8 eV. We see that excellent agreement is obtained between the experimental and theoretical results for all the cases.

It is interesting to compare the emission spectra and relative intensities for the junctions with different metal electrodes, $Si/SiO_2/Au$ and $Si/SiO_2/Al$, and for the two bias polarities. The comparison is shown in Fig. 7. Figure 7(a) shows the experimental data and Fig. 7(b) shows the calculated results. We see that the experimental spectra are well reproduced by the theory. Moreover, the relative strengths of the overall intensities for the different junctions and for the different bias polarities are very well reproduced theoretically. Since the absolute sensitivity of

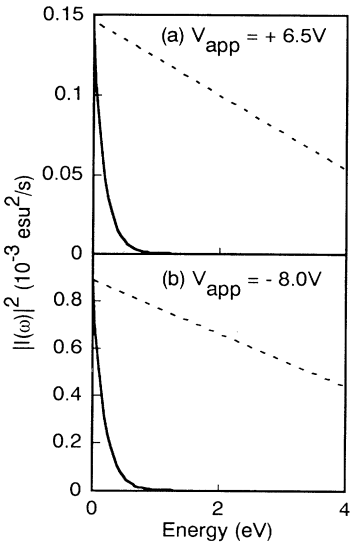

FIG. 6. Calculated current fluctuation spectra for the $Si/SiO_2/Al$ junction. (a) is for $V_{app}=+6.5$ V and (b) is for $V_{app}=-8.0$ V. The solid curves and the dashed curves are obtained by Eqs. (12) and (20), respectively.

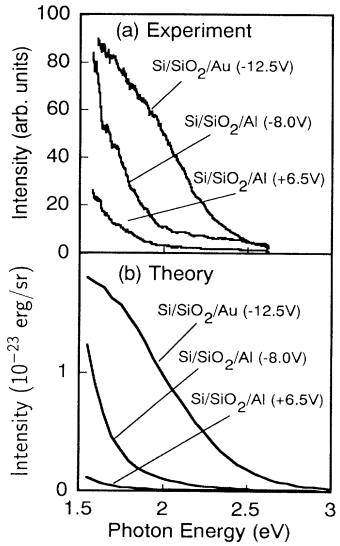

FIG. 7. Comparison of the emission spectra and the relative intensities for the junctions with different metal electrodes and for the two bias polarities. (a) and (b) correspond to the experimental and theoretical results, respectively.

our optical system is not calibrated, we could not compare the absolute intensities in Figs. 7(a) and 7(b). However, apart from the absolute calibration of the intensity axis, the agreement seen in Fig. 7 is remarkable.

V. DISCUSSION

Now let us discuss the light-emission mechanism of the Si-MOS junctions. Both Eqs. (1) and (2) can be divided into two parts as follows:

$$\frac{dW}{d\Omega\, d\omega\, dt}=\{A_d(\omega,d_j,\varepsilon_j)+A_r(\omega,d_j,\varepsilon_j,\zeta_j)\}|I(\omega)|^2 . \tag{19}$$

$A_d(\omega,d_j,\varepsilon_j)$ and $A_r(\omega,d_j,\varepsilon_j,\zeta_j)$ depend on the geometrical structure (d_j and ζ_j) and the dielectric properties (ε_j) of the junction, but do not depend on the bias voltage across the barrier. We call $A_d(\omega,d_j,\varepsilon_j)$ the antenna factor for the direct emission and $A_r(\omega,d_j,\varepsilon_j,\zeta_j)$, which is proportional to δ^2, the antenna factor for the roughness-mediated emission. The power spectrum of the current fluctuation, $|I(\omega)|^2$, depends on the bias voltage across the barrier and the properties of the tunneling barrier.

Let us consider the junction-dependent spectral shapes of $|I(\omega)|^2$ first and then the antenna factors separately. A linear dependence of $|I(\omega)|^2$ on frequency ω is often assumed in the theoretical calculations of LETJ's:[2,7]

$$|I(\omega)|^2=\begin{cases} eI_0\left[1-\dfrac{\hbar\omega}{eV_0}\right], & \hbar\omega<eV_0 , \\ 0, & \hbar\omega>eV_0 \end{cases} \tag{20}$$

where I_0 is the tunneling current and V_0 is the bias voltage across the tunneling barrier. The dashed lines in Fig. 6 are the plots of $|I(\omega)|^2$ obtained from Eq. (20) for the two biasing polarities. We recall that the solid curves are the plots of Eq. (12), which is based on the WKB approximation, and the solid curves are supposed to be more realistic than the dashed curves. We see that the linear approximation given by Eq. (20) is very poor for the junction parameters relevant to the present work. The reason for this difference between the two approximations can be easily understood. Equation (20) holds only for the limiting case of a very thin tunneling barrier and for a very low bias voltage.[7] On the other hand, the barrier thickness of our Si-MOS junctions was not very thin (around 6 nm) and the bias voltage was not very low; i.e., in the Fowler-Nordheim regime. Thus the comparison shown in Fig. 6 suggests that the linear approximation for $|I(\omega)|^2$ given by Eq. (20) is inappropriate for our junctions. If we had adopted Eq. (20) instead of Eq. (12) in calculating $|I(\omega)|^2$ no agreement between the theory and the experiments would have been achieved.

As seen from Fig. 6 the power spectra of the current fluctuation have similar shapes for $V_{\rm app}=+6.5$ and -8.0 V. Since the antenna factors do not depend on the bias voltage, the calculated emission spectra also have similar shapes for the two bias conditions. This result is in agreement with the observed results in Figs. 4(a) and 4(b).

Next we consider the spectral shape of the antenna factors. To evaluate the antenna factors, we need to estimate the scale of the roughness in the junction. The value of the autocorrelation distance a that is relevant to the light-emission process can be estimated from the following consideration. The strength of the electric field excited by the tunneling electrons $|E(\mathbf{Q}_p,\omega|z)|^2$ for a unit interval of $|\mathbf{Q}_p|$ is a function of the wave vector $\mathbf{Q}_p$ parallel to the surface, the mode frequency ω, and the observation position z. It is calculated by the following equation as described in the Appendix:

$$|E(\mathbf{Q}_p,\omega|z)|^2=A\frac{\omega^2}{c^4}\int dz'dz''\sum_{\mu=x,y,z} d_{\mu z}(\mathbf{Q}_p,\omega|zz')^* d_{\mu z}(\mathbf{Q}_p,\omega|zz')\frac{\Delta(z,z')}{(1+\mathbf{Q}_p^2\xi_0^2)^{3/2}}(2\pi|\mathbf{Q}_p|) . \tag{21}$$

Figures 8(a) and 8(b) show the contour maps of the strength of the electric field for the $Si/SiO_2/Al$ and $Si/SiO_2/Au$ junctions, respectively, at $z=z_{n-1}^+$ (at the top surface). We see high-field regions (in the $\omega,|\mathbf{Q}_p|$ plane) in both Figs. 8(a) and 8(b) that correspond to the SPP mode localized at the SiO_2/Al and SiO_2/Au interfaces (slow mode), respectively. The dashed lines in Fig. 8 are the dispersion curves of external light in vacuum ($\omega=ck$). The slow mode has a larger wave vector than that of the light of the same frequency; thus it is nonradiative. The size of wave-vector mismatch (Δk) between the slow mode and the external light is estimated from Fig. 8 to be $\Delta k\sim 0.4\times 10^6$ cm^{-1} around the photon energy of 2 eV. In order to scatter the SPP with wave vector $\mathbf{Q}_p$ into the external light with wave vector $\mathbf{k}_p$, the autocorrelation distance a must satisfy the condition

$$\tfrac{1}{4}a^2|\mathbf{k}_p-\mathbf{Q}_p|^2\le 1 \tag{22}$$

from wave-vector conservation. This means that a must be less than ~ 50 nm for efficient scattering of the SPP into the external light. Thus we have assumed that a is 20 nm.

The root-mean-squared amplitude of roughness δ can be estimated from the observed polarization characteristics of the emitted light. From Eq. (19) the polarization ratio of the s-polarized light to the p-polarized light is given by

$$\frac{I_{s\ \rm pol}}{I_{p\ \rm pol}}=\frac{A_r(\omega,d_j,\varepsilon_j,\zeta_j)_{s\ \rm pol}}{A_d(\omega,d_j,\varepsilon_j)_{p\ \rm pol}+A_r(\omega,d_j,\varepsilon_j,\zeta_j)_{p\ \rm pol}} . \tag{23}$$

Direct emission does not occur for s polarization. The right-hand side of Eq. (23) is zero for $\delta=0$, and increases up to the asymptotic value of

$$A_r(\omega,d_j,\varepsilon_j,\zeta_j)_{s\ \rm pol}/A_r(\omega,d_j,\varepsilon_j,\zeta_j)_{p\ \rm pol}$$

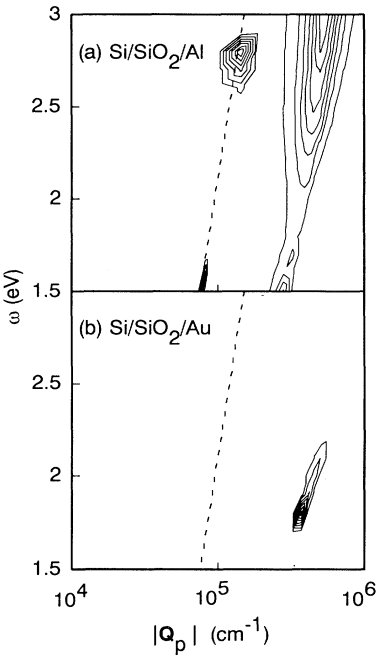

FIG. 8. Contour map of the electric-field strength at the surface of the $Si/SiO_2/Al$ junction (a) and the $Si/SiO_2/Au$ junction (b). The dashed line is the dispersion relation of light in vacuum. The maximum value of $|E(\mathbf{Q}_p,\omega|z)|^2$ for the $Si/SiO_2/Au$ junction is 49 times greater than that for the $Si/SiO_2/Al$ junction.

with increasing δ. Figure 9 shows the plots of Eq. (23) as a function of δ for $a=20$ nm for the $Si/SiO_2/Al$ junction. Here the scale of roughness was assumed to be the same at all interfaces and at the top surface. The polarization ratio increases from 1% for $\delta=1$ nm to 5% for $\delta=4$ nm. As we have noted earlier, the observed s/p ratio for the $Si/SiO_2/Al$ junction is $\frac{1}{55}$. Thus one can expect that δ is in the range between 1 and 2 nm for the $Si/SiO_2/Al$ junction.

In the estimation of the roughness described above, we assumed that the roughness at all the interfaces and the top surface has the same amplitude and autocorrelation distance. Then the dominant contribution to the light emission comes from the roughness at the interface of the oxide layer and the metal layer.[3] Since we used the same batch of Si substrates and used the same process for both types ($Si/SiO_2/Al$ or $Si/SiO_2/Au$) of the Si-MOS junctions before the final step (evaporation of the metal electrode), we expect that the roughness at the interfaces on the two sides of the oxide layer is the same for both types of junctions.

For the $Si/SiO_2/Au$ junction the calculated spectral shape is sensitive to the value of δ and the best fitting between the experimental and theoretical spectra is obtained at $\delta=1.3$ nm. Thus we assumed that $a=20$ nm and $\delta=1.3$ nm in the above theoretical calculation. These are very reasonable values from the above considerations.

Although the current fluctuation spectra and the roughness for the $Si/SiO_2/Al$ and $Si/SiO_2/Au$ junctions are similar, the spectral shapes of the two types of junctions are appreciably different as seen from Figs. 4 and 5. The origin of this difference lies in the difference in the SPP characteristics. Figures 10(a) and 10(b) illustrate the direct and roughness-mediated emission intensities separately for the $Si/SiO_2/Al$ junction biased at -8.0 V (a) and the $Si/SiO_2/Au$ junction at -12.5 V (b). For both types of junction the direct emission monotonically decreases toward the higher-energy side. This spectral feature arises from the spectral shape of the current fluctuation. A large difference is seen for the roughness-mediated emission spectra in the two junctions. The roughness-mediated emission from the $Si/SiO_2/Au$ junctions has a peak around 1.8 eV where the roughness-mediated emission is comparable to the direct emission. As we can see from Fig. 8 this peak is due to the slow mode of the SPP's. The maximum value of $|E(\mathbf{Q}_p,\omega|z)|^2$ for the $Si/SiO_2/Au$ junction is 49 times greater than that for the $Si/SiO_2/Al$ junction. Thus the roughness-

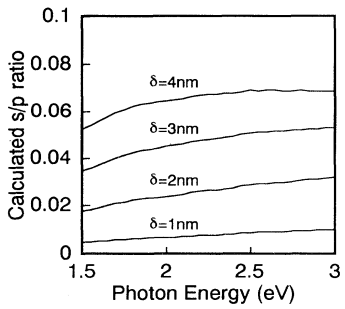

FIG. 9. Calculated polarization ratios as a function of δ for the $Si/SiO_2/Al$ junction of Fig. 4. The autocorrelation distance a is assumed to be 20 nm.

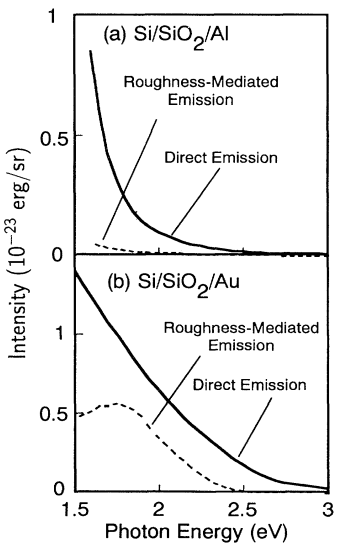

FIG. 10. Calculated direct emission spectra and roughness-mediated emission spectra shown separately. (a) for the $Si/SiO_2/Al$ junction and (b) for the $Si/SiO_2/Au$ junction.

mediated emission from the $Si/SiO_2/Al$ junction becomes small in comparison with that of the direct emission.

From the discussions above we can conclude that the light emitted from the $Si/SiO_2/Al$ junction is mainly due to the direct emission from the current fluctuation. On the other hand, nearly one-half of the emitted light from the $Si/SiO_2/Au$ junction is due to the direct emission and the other half is the indirect roughness-mediated emission from the SPP's.

VI. CONCLUSION

The visible-light-emission spectra observed from the $Si/SiO_2/Al$ and $Si/SiO_2/Au$ junctions were compared with the theoretical spectra calculated by the current fluctuation theory that incorporates a realistic power spectrum of the current fluctuation in the Fowler-Nordheim tunneling regime. The junction parameters were determined by electrical measurements of the individual junctions. Excellent agreement was achieved between the observed and the theoretically calculated spectra. We conclude that there are two channels of light emission, the direct channel and the roughness-mediated indirect channel. The emission from the $Si/SiO_2/Al$ junction is mainly due to the direct emission from the current fluctuation. On the other hand, the emission from the $Si/SiO_2/Au$ junction contains comparable contributions from both channels.

ACKNOWLEDGMENTS

Part of this work was carried out in the Laboratory for Microelectronics of our Institute. We thank T. Meguro of our Institute for making the photomasks for us. This research was supported in part by a Grant-in-Aid for Scientific Research from the Ministry of Education, Science, and Culture, and a grant from the Mitsubishi Foundation.

APPENDIX

The μ component of the electric field generated at position $\mathbf{x}$ by the tunneling current $J_z(\mathbf{x}',\omega)$ is calculated by use of the electromagnetic Green's function:[2]

$$E_\mu(\mathbf{x},\omega)=-\frac{\omega}{c^2}\int d^3x'\int\frac{d^2Q_p'}{(2\pi)^2}e^{i\mathbf{Q}_p'\cdot(\mathbf{x}_p-\mathbf{x}_p')}\times d_{\mu z}(\mathbf{Q}_p',\omega|zz')J_z(\mathbf{x}',\omega)\ . \tag{A1}$$

The electric field with wave vector $\mathbf{Q}_p$ is obtained from the Fourier transform

$$E_\mu(\mathbf{Q}_p,\omega|z)=\int d^2x_p E_\mu(\mathbf{x},\omega)e^{i\mathbf{Q}_p\cdot\mathbf{x}_p}\ . \tag{A2}$$

By substituting Eq. (A1) into (A2) we obtain

$$\begin{aligned}E_\mu(\mathbf{Q}_p,\omega|z)&=\int d^2x_p E_\mu(\mathbf{x},\omega)e^{i\mathbf{Q}_p\cdot\mathbf{x}_p}\\&=-\frac{\omega}{c^2}\int d^3x' e^{-i\mathbf{Q}_p\cdot\mathbf{x}_p'}\times d_{\mu z}(\mathbf{Q}_p,\omega|zz')J_z(\mathbf{x}',\omega)\ ,\end{aligned} \tag{A3}$$

where z is the z component of position $\mathbf{x}$. Then the (statistically averaged) strength of the electric field is given by

$$\begin{aligned}|E_\mu(\mathbf{Q}_p,\omega|z)|^2&=A\frac{\omega^2}{c^4}\int dz'dz''d_{\mu z}(\mathbf{Q}_p,\omega|zz')^*d_{\mu z}(\mathbf{Q}_p,\omega|zz'')J_{zz}(\mathbf{Q}_p,\omega|z'z'')\\&=\frac{\omega^2}{c^4}\int dz'dz''d_{\mu z}(\mathbf{Q}_p,\omega|zz')^*d_{\mu z}(\mathbf{Q}_p,\omega|zz'')\frac{1}{2\pi^2}\frac{\Delta(z,z')}{(1+\mathbf{Q}_p^2\xi_0^2)^{3/2}}|I(\omega)|^2\ ,\end{aligned} \tag{A4}$$

where A is the area of the junction. By summing (A4) for $\mu=x,y,z$ we obtain the strength of the electric field at z created by the fluctuating tunnel current. This is a general formula for the "power density" of the excited plasmons expressed by $P(\mathbf{k}_\parallel,\omega)$ in Refs. 3, 13, and 14.

When we discuss the characteristics of the roughness-mediated emission, it is important to know the $\mathbf{Q}_p$ dependence of $|E_\mu(\mathbf{Q}_p,\omega|z)|^2$ for each frequency ω. Since $|I(\omega)|^2$ decreases exponentially toward the high-frequency side, it is difficult to show clearly the $\mathbf{Q}_p$ dependence of $|E_\mu(\mathbf{Q}_p,\omega|z)|^2$ in the high-frequency region in a contour map in the Q_p-ω plane. Thus, instead of (A4), we plot a contour map of $|E(\mathbf{Q}_p,\omega|z)|^2$ defined by the following relation:

$$|E(\mathbf{Q}_p,\omega|z)|^2\equiv\frac{\omega^2}{c^4}\sum_{\eta=x,y,x}\int dz'dz''d_{\eta z}(\mathbf{Q}_p,\omega|zz')^*d_{\eta z}(\mathbf{Q}_p,\omega|zz'')\frac{1}{2\pi^2}\frac{\Delta(z,z')}{(1+\mathbf{Q}_p^2\xi_0^2)^{3/2}}(2\pi|\mathbf{Q}_p|)\ , \tag{A5}$$

where $2\pi|\mathbf{Q}_p|$ is the density of states of the SPP's for a unit interval of $|\mathbf{Q}_p|$ at wave vector $\mathbf{Q}_p$.

*Present address: Fujitsu Laboratories Ltd., 10-1 Morinosato-Wakamiya, Atsugi 243-01, Japan.

†Present address: Seiko Epson Corporation, 3-3-5 Owa, Suwa 392, Japan.

[1] J. Lambe and S. L. McCarthy, Phys. Rev. Lett. **37**, 923 (1976).

[2] B. Laks and D. L. Mills, Phys. Rev. B **20**, 4962 (1979).

[3] A. Takeuchi, J. Watanabe, Y. Uehara, and S. Ushioda, Phys. Rev. B **38**, 12 948 (1988).

[4] J. R. Kirtley, T. N. Theis, J. C. Tsang, and D. J. DiMaria, Phys. Rev. B **27**, 4601 (1983).

[5]J. Watanabe, Y. Uehara, and S. Ushioda, Jpn. J. Appl. Phys. **32**, 99 (1993).
[6]D. L. Mills and A. A. Maradudin, Phys. Rev. B **12**, 2943 (1975).
[7]D. Hone, B. Mühlschlegel, and D. J. Scalapino, Appl. Phys. Lett. **33**, 203 (1978).
[8]S. M. Sze, *Physics of Semiconductor Devices,* 2nd ed. (Wiley-Interscience, New York, 1981).
[9]M. A. Ordal, L. L. Long, R. J. Bell, R. R. Bell, R. W. Bell, R. W. Alexander, Jr., and C. W. Ward, Appl. Opt. **22**, 1099 (1983).
[10]P. B. Johnson and C. W. Christy, Phys. Rev. B **6**, 4370 (1972).
[11]D. F. Edwards, in *Handbook of Optical Constants of Solids,* edited by E. D. Palik (Academic, New York, 1985), p. 547.
[12]H. R. Philip, in *Handbook of Optical Constants of Solids* (Ref. 11), p. 719.
[13]S. Ushioda, J. E. Rutledge, and R. M. Pierce, Phys. Rev. B **34**, 6804 (1986).
[14]Zs. Szentirmay, Phys. Rev. B **36**, 2601 (1987).